Robustness Analysis of an L_1 Adaptive Controller

Peter Seiler*, Andrei Dorobantu† and Gary Balas‡
Department of Aerospace Engineering & Mechanics
University of Minnesota, Minneapolis, MN, 55455, USA

NASA's Generic Transport Model (GTM) is a remote-controlled, 5.5 percent scale commercial aircraft. An L_1 adaptive controller was recently designed and flight tested on the GTM. Oscillations in the elevator command were observed at 1.4 to 2 Hertz during the first flight test in September 2009. In most flight conditions the L_1 adaptive controller can be approximated by a linear time-invariant system. Thus linear analysis tools can be used to assess the performance and robustness of the feedback system with the L_1 controller. The initial L_1 design met the NASA requirement for 60 msec of time delay margin. However, the linear analysis indicates that the margin requirements were insufficient due to inaccurate models that were available at the time of the first flight test. A revised L_1 controller has significantly larger margins and demonstrated good performance during subsequent flight tests.

I. Introduction

NASA's Airborne Subscale Transport Aircraft Research (AirSTAR) program addresses the challenges associated with validating flight control laws in adverse conditions.[1,2] The Generic Transport Model (GTM) is the primary test aircraft for NASA's AirSTAR flight test facility.[3–6] The GTM is a remote-controlled, 5.5 percent scale commercial aircraft. The vehicle is dynamically scaled so that flight test results can be used to draw conclusions about the behavior of full-scale commercial aircraft. A high-fidelity six degree-of-freedom model of the GTM, called the GTM DesignSim, has also been developed.[7] Significant effort has been invested to model the GTM at flight conditions where nonlinear effects are significant,[5,6,8] e.g. post-stall.

Recently an L_1 adaptive controller with piecewise constant adaptive laws was designed for the GTM.[9,10] Additional details concerning this control strategy can be found in Refs. 10 and 11. The basic architecture of this controller consists of a state predictor, parameter adaptation law, and feedback control law. All three components are linear and thus the L_1 design described in Ref. 9 is a linear control law. The controller implementation that was flight tested includes several additional features not described in Ref. 9. These features include a single scalar gain-scheduled variable, integrator resets for L_1 initialization, and models of actuator saturation and delay. The scalar gain-scheduled variable is used to improve performance and provide different performance at different flight conditions. Low pass filters and the adaptation rate, which is the sampling rate of the piecewise constant adaptive law, are not gain-scheduled. In most flight conditions the nonlinear/time-varying effects of these additional features are negligible. The key point is that the flight-tested implementation of this L_1 adaptation law can be approximated as a linear time-invariant system. As a result it is possible to apply classical linear analysis tools to study the robustness of the closed-loop flight dynamics.

The L_1 adaptive controller with piecewise constant adaptive laws was flight tested in September 2009. Oscillations in the elevator command were observed at 1.4 to 2 Hz during the flight test. This paper uses linear analysis to study the performance of the longitudinal axis control law. The linear analysis indicates that the initial L_1 design had insufficient stability margins. Several effects were poorly modeled at the time of the initial design including the actuator dynamics and network delays. The linear analysis performed in this paper uses updated actuator and network models. The L_1 controller was re-designed using the more

*Senior Research Associate: seiler@aem.umn.edu.
†Graduate Student: dorob002@umn.edu.
‡Professor: balas@aem.umn.edu.

accurate updated models. This revised L_1 controller has significantly larger margins and was successfully flown during tests in March and June 2010.

The remainder of the paper has the following structure. First, results from the flight test in September 2009 are briefly reviewed in Section II. The linear models for the GTM and L_1 adaptive controllers are described in Section III. The linear analysis of the closed-loop system is given in Section IV. Conclusions are provided in Section V.

II. Review of Flight Test Results

This section briefly reviews the results from the flight test in September 2009. The flight test was performed using Version 7 of the L_1 adaptive controller. The GTM has inboard and outboard elevators on the left and right side of the aircraft. The same command was used for all four elevators during the test. The left subplot of Figure 1 shows the left outboard elevator command for 30 seconds prior to and after the engagement of the L_1 controller. The solid vertical line at $t = 533.62$ sec marks the turn-on time for the L_1 controller. The right subplot of Figure 1 zooms in on the elevator command for a five second window around the L_1 turn-on time. The displayed data is sampled at 60 Hz [a]. In both plots there is a noticeable increase in elevator command energy after the L_1 controller is engaged.

Figure 2 shows single-sided FFTs of the left outboard elevator command for 30 seconds prior to and after the engagement of the L_1 controller. The 30 second data window was chosen because an additional test signal was injected into the elevator command roughly 30 seconds after the engagement of the L_1 controller. The elevator command has an increase energy at higher frequencies (beyond 1.4 Hz) after the L_1 is turned on. In particular, there is a large increase in energy from 1.4 to 2 Hz. The 1.4 to 2 Hz oscillations in the elevator command will be the main focus for the remainder of this paper.

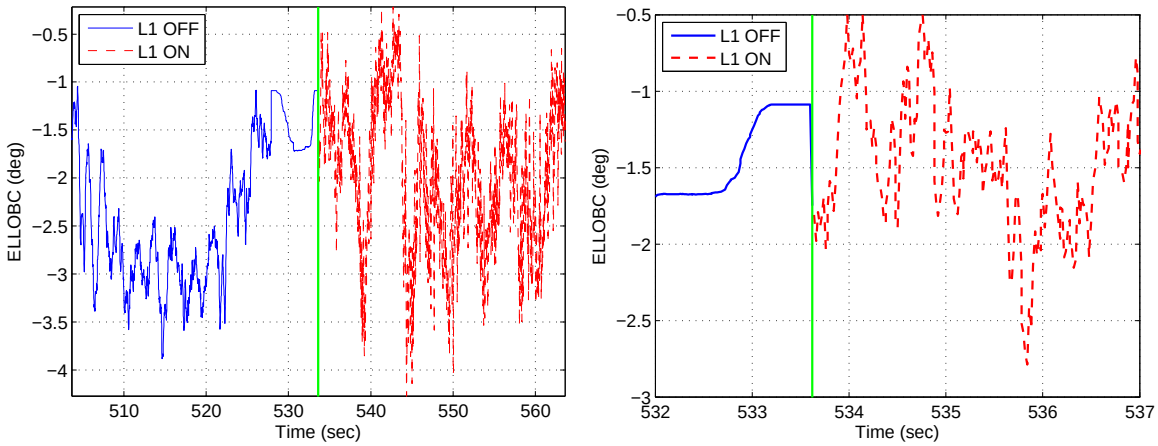

Figure 1. Time response of left outboard elevator command before and after engagement of L_1 controller

III. Model Development

The analysis models for the GTM aircraft and L_1 adaptive controller are described in this section. The development focuses on the longitudinal axis.

A. GTM Longitudinal Model

The main GTM aircraft parameters are provided in Table 1. NASA constructed a high fidelity 6 degree-of-freedom Simulink model of the GTM with the aerodynamic coefficients described as look-up tables.[6,7] This high fidelity simulation is referred to as the GTM DesignSim. This section describes a simplified four-state

[a]Data made available for this paper was provided at 60 Hz but was logged at a higher rate by NASA.

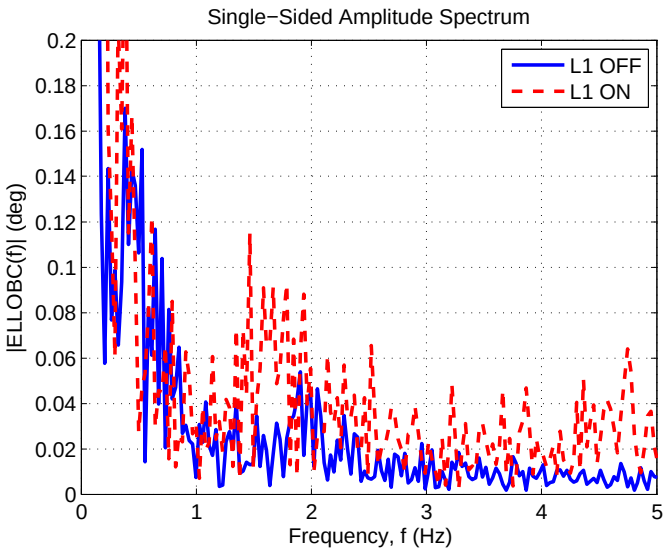

Figure 2. FFT of left outboard elevator command before and after engagement of L_1 controller

model of the GTM longitudinal dynamics. The parameter values are taken from the December 2009 (v0912) version of the GTM DesignSim.

Table 1. Aircraft and Environment Parameters

Wing Area, S	5.902 ft^2
Mean Aerodynamic Chord, $\bar{c}$	0.9153 ft
Mass, m	1.616 slugs
Pitch Axis Moment of Inertia, I_{yy}	4.253 slugs-ft^2
Air Density, ρ	0.002377 slugs/ft^3
Gravity Constant, g	32.17 ft/s^2

The longitudinal dynamics of the GTM are described by a standard four-state longitudinal model:[12]

$$\dot{V} = \frac{1}{m}\left(-D - mg\sin\left(\theta - \alpha\right) + T_x\cos\alpha + T_z\sin\alpha\right) \tag{1}$$

$$\dot{\alpha} = \frac{1}{mV}\left(-L + mg\cos\left(\theta - \alpha\right) - T_x\sin\alpha + T_z\cos\alpha\right) + q \tag{2}$$

$$\dot{q} = \frac{\left(M + T_m\right)}{I_{yy}} \tag{3}$$

$$\dot{\theta} = q \tag{4}$$

where V is the true air speed (knots), α is the angle of attack (deg), q is the pitch rate (deg/s) and θ is the pitch angle (deg). The control inputs are the elevator deflection δ_{elev} (deg) and engine throttle δ_{th} (percent).

The drag force D (lbs), lift force L (lbs), and aerodynamic pitching moment M (lb-ft) are given by:

$$D = \bar{q}SC_D(\alpha, \delta_{elev}, \hat{q}) \tag{5}$$

$$L = \bar{q}SC_L(\alpha, \delta_{elev}, \hat{q}) \tag{6}$$

$$M = \bar{q}S\bar{c}C_m(\alpha, \delta_{elev}, \hat{q}) \tag{7}$$

where $\bar{q} := \frac{1}{2}\rho V^2$ is the dynamic pressure (lbs/ft^2) and $\hat{q} := \frac{\bar{c}}{2V}q$ is the normalized pitch rate (unitless). C_D, C_L, and C_m are unitless aerodynamic coefficients computed from look-up tables provided by NASA. NASA provides raw look-up table data for the aerodynamic coefficients in the airframe body axes, i.e. the raw data

is provided for C_X, C_Z, and C_m.[b] The body-axis look-up tables C_X and C_Z were transformed into lift and drag coordinates via a rotation of angle α about the lateral axis.

The GTM has engines on the port and starboard sides of the airframe. Thrust settings for both engines were equal during the flight test. The thrust from a single engine T (lbs) is a function of the throttle setting δ_{th} (percent). $T(\delta_{th})$ is specified as a ninth-order polynomial in NASA's high fidelity GTM DesignSim. T_x (lbs) and T_z (lbs) denote the projection of the total engine thrust along the body x-axis and body-z axis, respectively. T_m (lbs-ft) denotes the pitching moment due to both engines. T_x, T_z and T_m are given by:

$$T_x(\delta_{th}) = n_{ENG} T(\delta_{th}) \cos(\epsilon_2) \cos(\epsilon_3) \tag{8}$$

$$T_z(\delta_{th}) = n_{ENG} T(\delta_{th}) \sin(\epsilon_2) \cos(\epsilon_3) \tag{9}$$

$$T_m(\delta_{th}) = r_z T_x(\delta_{th}) - r_x T_z(\delta_{th}) \tag{10}$$

$n_{ENG} = 2$ is the number of engines. $\epsilon_2 = 1.98$ deg and $\epsilon_3 = 2.22$ deg specify the rotation from engine axes to the airplane body axes. $r_x = 0.4406$ ft and $r_z = 0.3336$ ft specify the moment arm of the thrust.

The L_1 adaptive controller was tested at approximately $V = 80$knots. At this speed the level flight trim condition for the longitudinal dynamics is:

$$x_t := \begin{bmatrix} V_t \\ \alpha_t \\ q_t \\ \theta_t \end{bmatrix} = \begin{bmatrix} 80.00 \text{ knots} \\ 4.18 \text{ deg} \\ 0 \text{ deg/s,} \\ 4.18 \text{ deg} \end{bmatrix}, \; u_t := \begin{bmatrix} \delta_{th,t} \\ \delta_{elev,t} \end{bmatrix} = \begin{bmatrix} 19.37\% \\ 1.74 \text{ deg} \end{bmatrix} \tag{11}$$

The subscript "t" denotes a trim value. Linearizing around this trim point gives the following linear, time-invariant (LTI) model for the longitudinal dynamics:

$$\dot{\delta x} = \begin{bmatrix} -0.0451 & -0.0876 & -0.0007 & -0.3327 \\ -0.3401 & -2.8083 & 0.9489 & 0 \\ -0.4963 & -42.6565 & -3.6384 & 0 \\ 0 & 0 & 1.0 & 0 \end{bmatrix} \delta x + \begin{bmatrix} 0.0788 & -0.0263 \\ -0.0022 & -0.2809 \\ 0.8675 & -45.9280 \\ 0 & 0 \end{bmatrix} \delta u \tag{12}$$

where $\delta x := x - x_t$ and $\delta u := u - u_t$.

There are several components that must be modeled in addition to the basic airframe dynamics. One important feature of the GTM platform is that measurements are transmitted down to a ground station. The control laws are computed at the ground station and then transmitted back to the GTM. The additional dynamics from measurement to actuation can have a significant effect of the robustness of the feedback loop. The following effects were included in the LTI longitudinal model:

1. **Sensors**: The pitch rate measurement is generated by the MAG3 sensor. A specially ordered 200 Hz bandwidth MAG3 was originally used on the GTM but this was replaced for the September 2009 flight test by a standard MAG3 with 50 Hz bandwidth. The pitch rate sensor is modeled as a first-order transfer function with a 50 Hz bandwidth. Vibration isolation was installed for the MAG3 between the September 2009 and March 2010 flight tests. This introduced 6 msec of lag in the MAG3 measurements for the March 2010 test. This additional 6 msec lag is modeled as a time delay for the analysis of the March 2010 test but it is not included for the analysis of the September 2009 test.

   The Air Data sensor measures angle of attack and total pressure. Total pressure is turned into airspeed by a nonlinear function. This nonlinear function is neglected in the analysis and the Air Data sensor is modeled as directly sensing airspeed. No dynamic model of the air data sensor is included in the GTM DesignSim. It is assumed that these sensor dynamics are negligible. Both sensors have scale factor and bias errors. These errors are neglected in the linear analysis. The pitch angle measurement is generated by the MIDG II sensor. The MIDG II sensor dynamics are neglected since the pitch angle is not used for feedback in this analysis.

2. **Anti-Aliasing Filters**: Anti-aliasing filters for pitch rate, angle of attack, and airspeed measurements are modeled as first order transfer functions with time constants of 10 msec (bandwidth = 15.9 Hz).

[b]The notation refers to standard aircraft body axis conventions.[12] x is directed to the front along the longitudinal axis of the aircraft and z is directed down. X and Z are the aerodynamic forces along the x and z axes, respectively.

3. **Downlink**: The downlink is modeled as a 6 msec delay. This includes queuing delays, transmission time, and delays due to asynchronous timing of subsystem components.

4. **Processor**: The processor runs at 600 Hz. It is assumed that the processor takes the entire sample time to compute the controller. The processor is modeled as one sample ($T_s \approx 1.667$ msec) of delay.

5. **Uplink**: The uplink is modeled as a 15 msec delay. This includes queuing delays, transmission time, and delays due to asynchronous timing of subsystem components. The processor and uplink delays are lumped as a single delay at the plant input.

6. **Actuators**: The elevator actuator is modeled as a first order system with 5 Hz bandwidth and 10 msec of pure time delay. The actuator has several nonlinear effects including backlash and hysteresis. These nonlinear effects are not modeled in the linear analysis. The throttle lag is modeled as the second order system $\frac{-0.147s + 0.731}{s^2 + 1.34s + 0.731}$.

There are two important points to note concerning this analysis model. First, an older version of the GTM DesignSim (v0905) modeled the elevator actuator with a 10 Hz bandwidth and zero delay. The L_1 controller tested in September 2009 was designed based on this older, less accurate actuator model. This L_1 controller was designed to meet the NASA requirement for 60 msec of time delay margin based on the inaccurate models that were available at the time. However, the lower bandwidth and additional delay in the actual elevator model has a significant impact on the actual (as compared to the designed) stability margins. Second, wind turbulence is not modeled and this was a factor during some flight tests. It would be possible to use linear analysis to investigate the effect of turbulence. This paper focuses on stability margins and thus the effect of turbulence on performance is not considered.

B. Longitudinal-Axis L1 Adaptive Controller

This section briefly reviews the architecture of the L_1 adaptive controller with piecewise constant adaptive laws designed for the GTM. Full details on the design of this controller are provided in Ref. 9. Additional theoretical details and applications of the L_1 adaptive controller with piecewise constant adaptive laws are given in Refs. 10 and 11. This section focuses on the longitudinal axis of the L_1 controller. The architecture is similar for the lateral axis. Two versions of the L_1 controller will be analyzed in this paper. Version 7 was flight tested in September 2009 and exhibited the 1.4 to 2 Hz oscillations in the elevator command shown in Figure 2. Version 12 was successfully flight tested in March 2010 without the oscillations in the elevator channel. The two versions use the same architecture with minor differences in implementation. All controller parameters (e.g. adaptation gains, filter time constants) were obtained from the Simulink implementations for the two L_1 adaptive controllers.

The longitudinal controller design assumes the short period dynamics of the GTM can be modeled as:

$$\dot{x}(t) = A_m x(t) + B_m \left(u(t) + f_1(x(t), t)\right) + B_{um} f_2(x(t), t) \tag{13}$$

$$y(t) = Cx(t) \tag{14}$$

where $x := [\alpha,\ q]^T$ and $u := \delta_{elev}$. $y := \alpha$ is the regulated output. A_m and B_m define the desired short period dynamics. f_1 and f_2 are unknown matched and unmatched uncertainties that represent the difference between the actual and desired short period dynamics. The derivation in Ref. 9 also allows for internal unmodeled dynamics but this generalization has been neglected for simplicity.

The longitudinal L_1 adaptive control law is designed to track an angle of attack command from the pilot. Specifically, the goal is to have the regulated output $y(t) := \alpha(t)$ track the desired response $y_m(t)$ due to a reference command $r(t) := \alpha_{cmd}(t)$ from the pilot. The desired response is given by the reference model:

$$\dot{x}_m = A_m x_m(t) + B_m K_g r(t) \tag{15}$$

$$y_m(t) = Cx_m(t) \tag{16}$$

The feedforward gain is chosen to be $K_g = -(CA_m^{-1}B_m)^{-1}$ so that the response from $r(t)$ to $y_m(t)$ has a steady state gain of one.

The L_1 adaptive control law uses state feedback to accomplish this tracking objective. The basic idea is to estimate the effect of the matched and unmatched uncertainties on the output $y(t)$. The controller attempts

to compensate for these uncertainties up to a defined bandwidth. The bandwidth is set by low-pass filters introduced into the controllers. These low-pass filters provide separation between adaptation and robustness as well as attenuating high frequency content in the controller output $u(t)$. This is important because L_1 designs typically use large adaptation gains which lead to high frequency content in some of the internal states of the controller.

Figure 3 shows the high-level structure of the L_1 adaptive controller. The controller inputs are the reference command r and the measurements of the short period state x. The output is the elevator command u. The architecture consists of three components:

1. **State Predictor:**

$$\dot{\hat{x}} = A_m\hat{x} + B_m\left(u + \hat{\sigma}_m\right) + B_{um}\hat{\sigma}_{um} \tag{17}$$

$\hat{\sigma}_m$ and $\hat{\sigma}_{um}$ are estimates of the matched and unmatched uncertainties. These are computed by an adaptive law. $\hat{x}$ is the estimate of the short period states $x = [\alpha,\ q]^T$. $\hat{x}$ is an open-loop state prediction, i.e. it does not use state measurements to correct the estimate. Instead, the difference between the open-loop state estimate $\hat{x}(t)$ and the measured state $x(t)$ is used by the adaptive law to update the estimates of the model uncertainty.

2. **Adaptive Laws:** The estimates of the model uncertainties are updated with a piecewise-constant adaptive law:

$$\begin{bmatrix}\hat{\sigma}_m(t)\\ \hat{\sigma}_{um}(t)\end{bmatrix} = M\tilde{x}(kT_s) \qquad \forall t \in [kT_s, (k+1)T_s] \tag{18}$$

where $\tilde{x}(t) = \hat{x}(t) - x(t)$ is the state estimation error and T_s is the sampling rate. M is the constant matrix defined as $M := -[B_m,\ B_{um}]^{-1}\Phi^{-1}(T_s)e^{A_mT_s}$ where $\Phi(T_s) := A_m^{-1}(e^{A_mT_s} - I)$. This adaptive law samples $\tilde{x}$ every T_s seconds and updates the model uncertainty estimates. The sample time is $T_s = 1.667$ msec. The sample rate is fast relative to the short period dynamics and hence the adaptive law is essentially a continuous-time constant matrix gain.

3. **Control Law:** The elevator command is generated as:

$$u = -C_1(s)\hat{\sigma}_m - C_2(s)H_1^{-1}(s)H_2(s)\hat{\sigma}_{um} + K_g r \tag{19}$$

where $H_1(s) := C(sI - A_m)^{-1}B_m$ and $H_2(s) := C(sI - A_m)^{-1}B_{um}$ are the transfer functions from the matched and unmatched uncertainty to the output, respectively. $C_1(s)$ and $C_2(s)$ are low pass filters chosen to attenuate the high frequency content in the model uncertainty estimates. The first term of this control law attempts to compensate for the matched model uncertainty up to the bandwidth of $C_1(s)$. $H_2(s)\hat{\sigma}_{um}$ estimates the effect of the unmatched uncertainty on the model output and $H_1^{-1}(s)H_2(s)\hat{\sigma}_{um}$ is the input needed to cancel the effect of this uncertainty at the output. Thus the second term in the control law attempts to cancel the effect of the unmatched uncertainty up to the bandwidth of $C_2(s)$. The last term in $u(t)$ is the reference angle of attack with the desired gain.

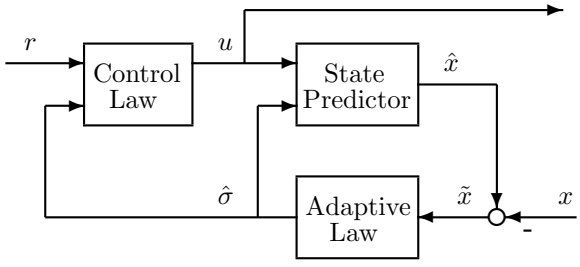

Figure 3. Architecture for L_1 Adaptive Controller

All three components of the L_1 adaptive controller with piecewise constant adaptive laws are essentially linear time-invariant systems. The state predictor is just a linear state-space system. The adaptive law

consists of a sample/hold and a constant matrix gain. This can be represented as a continuous-time, constant matrix gain for the fast sample rate used by the controller. Finally, the control law component consists of low pass filters, transfer functions modeling the effect of the unmatched uncertainties, and a constant gain. This control law component is a three-input, one-output linear time-invariant system. To summarize, the L_1 adaptive controller described in Ref. 9 can be well-approximated by a linear time-invariant system. This conclusion is in contrast to most adaptive laws which use nonlinear terms in both the the adaptive law and the control law. For example, other variants of L_1 adaptive control[13] and most variants of model reference adaptive control contain quadratic terms in both the adaptive law and the control law. The L_1 adaptive controller with piecewise constant adaptive laws can also be implemented using integral (nonlinear) projection-type adaptive laws.[13]

The flight tested L_1 adaptive controllers are implemented in Simulink. The Simulink implementation includes several additional features not described in Ref. 9. First, a single scalar gain on the B-matrix is scheduled to improve performance and provide different performance at different flight conditions. The scheduling is based on α and V and the scheduling variables are low-pass filtered. In the linear analysis the gain-schedule variable is assumed to be constant at their values for the flight condition $V = 80$knots and $\alpha = 6.5^o$. This is approximately the mean flight condition during the September 2009 flight test. Second, there is logic to reset all integrators when the controller is initially turned on. The reset logic is neglected in the linear analysis. Third, the reference angle-of-attack command is smoothed by a low-pass filter and a command pre-filter in addition to being multiplied by the gain K_g. These filters are included in the linear analysis. The fourth difference occurs in the implementation of the state predictor. The implemented state predictor differs from Equation 17 in that it includes a model of the actuator. Versions 7 includes models for the rate and magnitude saturation limits as well as a model for the network/actuator time delays. Version 12 includes updated values for the limits/delays and it also includes a first-order transfer function model for the actuator dynamics. As mentioned previously, Version 7 was designed using inaccurate actuator / network models while Version 12 was designed using the updated, more accurate models. The time delay and actuator dynamics are included in the linear analysis. However, it will be assumed that the effects of the actuator saturation model in the state predictor can be neglected. Finally, Version 12 also includes a pitch rate stability augmentation system in addition to the L_1 control law described above. In this version, the elevator command is $\delta_{elev,cmd} = -0.05q + u_{L1}$ where u_{L1} is the control command computed by the L_1 controller. The pitch rate feedback adds damping to the short period mode. Version 7 did not include this pitch rate feedback term. In summary, both versions of the L_1 adaptive controller contain numerous implementation details. However both versions can be reasonably approximated as linear time-invariant systems over a wide portion of the flight envelope.

C. Validation of Linear Model

A linear, time-invariant approximation for the closed loop system was constructed from the linearization of the GTM longitudinal dynamics and the LTI approximation for the L_1 controller. The longitudinal L_1 controller is designed to track angle of attack commands. During the September 2009 flight test the pilot controlled the throttle to maintain the airspeed. The pilot control of velocity is modeled with a simple proportional throttle controller: $\delta_{th} = \delta_{th,t} + K_{th}(V_t - V)$ with $K_{th} = 5$. A state space model of the closed loop system was constructed by connecting the L_1 and throttle controllers in feedback with the linear model of the longitudinal GTM dynamics.

To validate the approximation, the linear system was simulated with pulse angle-of-attack commands of various magnitudes. The results were compared with nonlinear simulation results using the GTM DesignSim. The nonlinear simulation included the high fidelity 6DOF GTM model and the flight tested implementation of the L_1 controller. The L_1 controller in the nonlinear simulation included both the longitudinal and lateral axes of the controller as well as all the special implementation features described at the end of the previous section. Figure 4 shows the responses of the linear and nonlinear simulations to a 2 deg angle of attack pulse command. Version 7 of the L_1 adaptive controller was used to generate the linear and nonlinear responses in this figure. The short period response of the linear model is similar to that of the nonlinear model. There are small differences in the long-period responses.

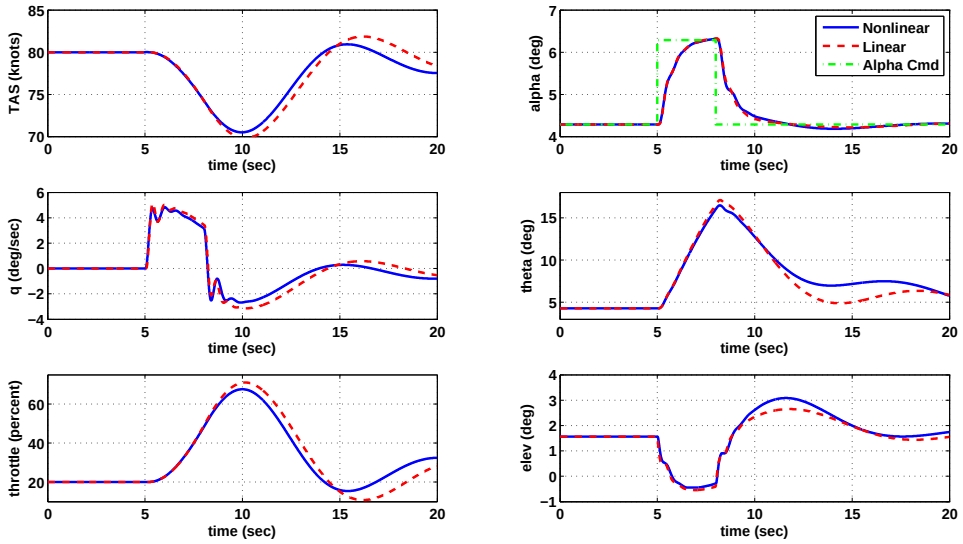

Figure 4. Nonlinear and linear closed-loop response to pulse α command

IV. Linear Analysis

The longitudinal axis of the L_1 controller has three inputs (α_{cmd}, α, and q) and one output ($\delta_{elev,cmd}$). The linear, time-invariant approximation for the L_1 controller allows the feedback system to be analyzed using a variety of linear analysis tools. For example, Figure 5 shows the Bode plots for Versions 7 and 12 of the longitudinal axis of the L_1 controller. The columns of Figure 5 are the Bode plots from α_{cmd}, α, and q, respectively to the $\delta_{elev,cmd}$. For both versions, the transfer function from α_{cmd} to $\delta_{elev,cmd}$ is approximately $-k/s$ at low frequencies for some constant k. The transfer function from α to $\delta_{elev,cmd}$ is approximately $+k/s$ at low frequencies for the same constant k. Thus the L_1 can be interpreted as having an integral control term on the α tracking error. This interpretation is only approximate however because both gains eventually level out to constant values at very low frequencies.

The effect of the pitch rate stability augmentation system in Version 12 is apparent in the Bode plot from q to $\delta_{elev,cmd}$ (third column of Figure 5). The approximately constant gain at low frequencies is the result of this additional feedback term. Version 7, on the other hand, has much lower gain especially from 1 to 10 rad/sec. At V=80knots, the short period mode of the GTM is at 7.12 rad/sec with a damping of 0.45. The additional stability augmentation system in Version 12 increases the pitch rate gain at the short period frequency and thus adds damping to this mode.

The Bode plot from α to $\delta_{elev,cmd}$ (middle column of Figure 5) has a significant increase in gain and phase starting around 5 rad/sec for both controllers. This appears to add phase lead to the feedback system. For Version 7, the gain of this transfer function exceeds 10 dB from 50 to 400 rad/sec and the gain exceeds 0 dB out to 1400 rad/sec. Thus the effect of α measurement noise on elevator command is amplified over a wide frequency band by Version 7. This might explain the increase in high frequency (beyond 2 Hz) energy in the elevator command shown in Figure 2. In Version 12 the α to $\delta_{elev,cmd}$ transfer function rolls off at a much lower frequency.

The performance of the feedback system can also be analyzed using the input loop transfer function. The input loop transfer function, denoted $L_I(s)$, is the scalar, open loop transfer function from the elevator input of the plant to the elevator output from the L_1 controller. The α_{cmd} input to the L_1 controller is neglected and the proportional throttle controller ($K_{th} = 5$) is wrapped in feedback around the longitudinal dynamics. As mentioned previously this proportional control roughly models the pilot control of the throttle. The results reported in the remainder of the section are similar for a wide range of throttle gains ($K_{th} \geq 2$). The Bode plot of the input loop transfer function is shown in Figure 6. This figure shows that Version 12 has a significantly lower bandwidth than Version 7. It is also important that Version 7 crosses 0 dB near 8.4 rad/sec and there is a very sharp roll-off in phase occurring at this frequency. As a result, small increases in loop gain, e.g. due to scale factor errors in the sensors, can drastically reduce the phase margin of Version

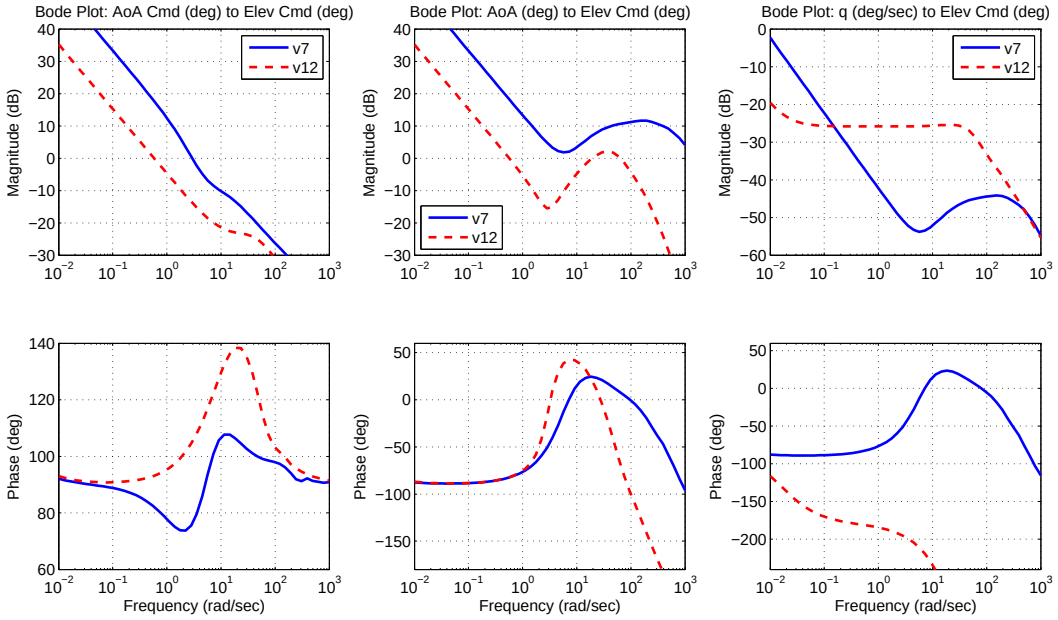

Figure 5. Bode Plots for Version 7 (v7) and Version 12 (v12) of the L_1 controller

7. This is important because scale factor errors in the α measurement, attributed to upwash on the sensor, were observed during flight tests.

Stability margins for both versions of the L_1 control law can be computed using the input loop transfer function. The first three rows of Table 2 shows the classical gain, phase, and delay margins. These classical margins measure robustness with respect to either gain or phase variations. The last two rows of Table 2 are robustness margins that allow for simultaneous gain and phase variations. The fourth row shows the disk margin. The disk margin defines the largest disk that encircles -1 and does not intersect the Nyquist plot of $L_I(j\omega)$.[14–16] The disk margin disk passes through $-d$ and $-1/d$ where d denotes the disk margin. The disk margin defines a set of simultaneous gain and phase variations for which the system is stable. This set can be plotted with the Matlab function DMPLOT.[17] The fifth row of Table 2 gives the minimum distance from the Nyquist plot of L_I to the critical point at -1.

Version 7 has smaller gain and phase margins than Version 12. However, the gain/phase margins for Version 7 are not, on their own, indicative of a robustness issue. In fact the margins for Version 7 exceed the typical flight control requirements for a gain margin of at least 6 dB (gain ≈ 2) and 45^o of phase margin. The high bandwidth of Version 7 results in much higher gain and phase margin frequencies than for Version 12. This causes two issues. First, model uncertainties are typically larger at higher frequencies making it more likely that the system margins will be exceeded. Second, phase margins at higher frequencies correspond to smaller delay margins. This is evident in the third row of Table 2. Version 7 has a significantly smaller delay margin than Version 12. The last two rows of Table 2 show that Version 7 also has smaller stability margins than Version 12 with respect to the measures that allow for simultaneous phase and gain variations. In particular, for Version 7 the minimum distance from the Nyquist plot of L_I to the critical point is roughly half of that corresponding to Version 12. It should be noted that for Version 7 the frequencies for all stability margins occur between 8.42 and 14.49 rad/sec ($\approx$ 1.34 to 2.31 Hz). This is in agreement with the 1.4 to 2 Hz energy observed in the FFT of the elevator command (Figure 2).

The minimum distance to the critical point can be used to construct a destabilizing perturbation. For Version 7, the minimum distance to the critical point occurs at $\omega_c = 11.25$ rad/sec. At this frequency the input loop transfer function is $L_I(\omega_c) = -0.597 - 0.221i$ and $-1/L_I(\omega_c) = 1.473 - 0.544i = 1.57e^{-0.354i}$. $-1/L_I(\omega_c)$ can be rewritten as $1.57e^{-0.0315\omega_c i}$. Thus the feedback system will be destabilized by a simultaneous gain of 1.57 and delay of 31.5 msec at the elevator input. This gain/delay perturbation places two poles of the feedback system at $\pm 11.25i$. This perturbation was introduced into the nonlinear simulation to verify the results of the linear analysis. The nonlinear simulation again refers to the GTM DesignSim with

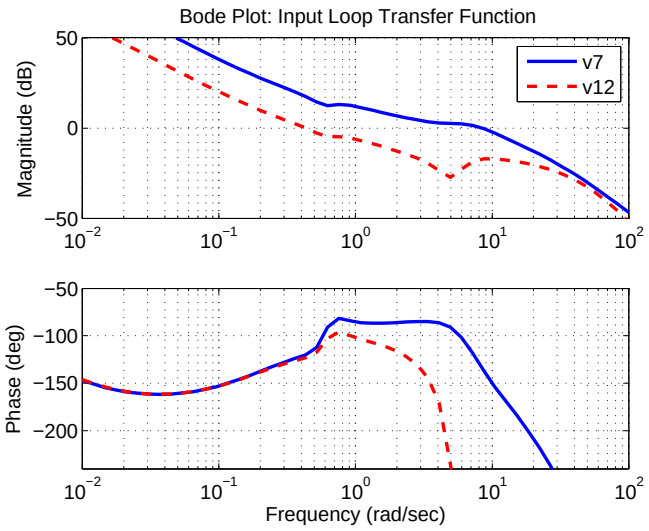

Figure 6. Bode plot of input loop transfer function for Version 7 (v7) and Version 12 (v12)

Table 2. Stability Margins

	Version 7 (Sept. 2009)	Version 12 (Mar. 2010)
Gain Margin	2.43 at 14.49 rad/sec	17.01 at 4.26 rad/sec
Phase Margin	46.3^o at 8.42 rad/sec	56.8^o at 0.43 rad/sec
Delay Margin	0.096 sec at 8.42 rad/sec	2.3 sec at 0.43 rad/sec
Disk Margin	1.79 at 10.8 rad/sec	3.18 at 0.35 rad/sec
$\min_\omega \lvert 1 + L_I(\omega)\rvert$	0.46 at 11.25 rad/sec	0.91 at 2.77 rad/sec

the high fidelity 6DOF model of the GTM and the full longitudinal/lateral implementations of Version 7 of the L_1 adaptive control law. The simultaneous gain of 1.57 and delay of 31.5 msec was introduced at elevator input to the plant. Figure 7 shows the system response to a 2^o pulse angle of attack command. The drop in velocity is due to the low-gain used for the proportional throttle control. The system has a pronounced oscillation at approximately 11 rad/sec (1.75 Hz). Again, this is in agreement with the 1.4 to 2 Hz energy observed in the FFT of the elevator command (Figure 2).

V. Conclusion

The L_1 adaptive controller with piecewise constant adaptive laws was approximated by a linear time-invariant system. This linear model was used to study the stability margins of the longitudinal axis of the L_1 controller. It was shown that the initial implementation of the L_1 controller had low stability margins. Moreover, the closest point from the Nyquist plot of the input loop transfer function to the critical point at -1 occurs approximately at 1.7 Hz. This is in agreement with 1.4 to 2 Hz oscillations in the elevator command that were observed during a flight test in September 2009. A revised L_1 controller has significantly larger stability margins and demonstrated good performance during subsequent flight tests in March and June 2010.

VI. Acknowledgments

This research was supported under the NASA Langley NRA contract NNH077ZEA001N entitled "Analytical Validation Tools for Safety Critical Systems". The technical contract monitor is Dr. Christine Belcastro. The authors gratefully acknowledge Irene Gregory, Naira Hovakimyan, and Enric Xargay for

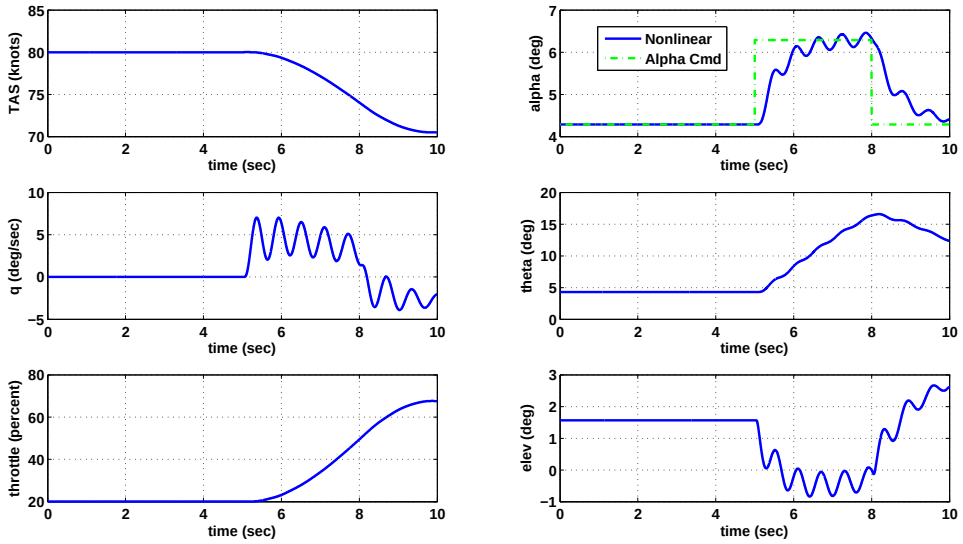

Figure 7. Nonlinear response to pulse α command with simultaneous gain/delay perturbation at δ_{elev} input

providing flight test data and the flight-tested implementations of the L_1 control laws. The authors also acknowledge Austin Murch for his input on modeling of the AirSTAR platform.

References

[1]A. Murch, "A flight control system architecture for the NASA AirSTAR flight test infrastructure," in *AIAA Guidance, Navigation and Control Conference and Exhibit, Honolulu, Hawaii*, 2008.

[2]A. Murch, D. E. Cox, and K. Cunningham, "Software considerations for subscale flight testing of experimental control laws," in *AIAA Infotech at Aerospace Conference and Exhibit, Washington, United States*, 2009.

[3]T. L. Jordan, J. V. Foster, R. M. Bailey, and C. M. Belcastro, "AirSTAR: A UAV platform for flight dynamics and control system testing," in *25th AIAA Aerodynamic Measurement Technology and Ground Testing Conference, San Francisco, CA*, no. AIAA 2006-3307, 2006.

[4]T. L. Jordan and R. M. Bailey, "NASA Langley's AirSTAR testbed: A subscale flight test capability for flight dynamics and control system experiments," in *AIAA Guidance, Navigation and Control Conference and Exhibit, Honolulu, Hawaii*, no. AIAA 2008-6660, 2008.

[5]R. Bailey, R. Hostetler, K. Barnes, C. M. Belcastro, and C. M. Belcastro, "Experimental validation: Subscale aircraft ground facilities and integrated test capability," in *AIAA Guidance, Navigation, and Control Conference and Exhibit, San Francisco, CA*, no. AIAA 2005-6433, 2005.

[6]A. Murch and J. Foster, "Recent NASA research on aerodynamic modeling of post-stall and spin dynamics of large transport airplanes," in *45th AIAA Aerospace Sciences Meeting and Exhibit, Reno, Nevada*, 2007.

[7]D. Cox, *The GTM DesignSim v0912*, 2009.

[8]J. Foster, K. Cunningham, C. M. Fremaux, G. Shah, E. Stewart, R. Rivers, J. Wilborn, and W. Gato, "Dynamics modeling and simulation of large transport airplanes in upset conditions," in *AIAA Guidance, Navigation, and Control Conference*, no. AIAA-2005-5933, 2005.

[9]I. M. Gregory, C. Cao, E. Xargay, N. Hovakimyan, and X. Zou, "$\mathcal{L}_1$ adaptive control design for NASA AirSTAR flight test vehicle," in *AIAA Guidance, Navigation, and Control Conference*, no. AIAA 2009-5738, 2009.

[10]E. Xargay, N. Hovakimyan, and C. Cao, "$\mathcal{L}_1$ adaptive controller for multi–input multi–output systems in the presence of nonlinear unmatched uncertainties," in *Proc. of the American Control Conference*, Baltimore, MD, 2010, pp. 874–879.

[11]T. Leman, E. Xargay, G. Dullerud, N. Hovakimyan, and T. Wendel, "$\mathcal{L}_1$ adaptive control augmentation system for the X-48B aircraft," in *AIAA Guidance, Navigation, and Control Conference*, no. AIAA 2009-5619, 2009.

[12]B. Stevens and F. Lewis, *Aircraft Control and Simulaion*. John Wiley & Sons, 1992.

[13]N. Hovakimyan and C. Cao, *$\mathcal{L}_1$ Adaptive Control Theory*. Philadelphia, PA: Society for Industrial and Applied Mathematics, 2010.

[14]M. Barrett, "Conservatism with robustness tests for linear feedback control systems," Ph.D. dissertation, University of Minnesota, 1980.

[15]J. Blight, R. Dailey, and D. Gangsass, "Practical control law design for aircraft using multivariable techniques," *International Journal of Control*, vol. 59, no. 1, pp. 93–137, 1994.

[16]D. Bates and I. Postlethwaite, *Robust Multivariable Control of Aerospace Systems*. Delft University Press, 2002.

[17]G. Balas, R. Chiang, A. Packard, and M. Safonov, *Robust Control Toolbox*, The MathWorks, 2009.